2010 IEEE International Conference on Robotics and Automation
Anchorage Convention District
May 3-8, 2010, Anchorage, Alaska, USA

Miniaturized Triaxial Optical Fiber Force Sensor for MRI-Guided Minimally Invasive Surgery

Pinyo Puangmali, Prokar Dasgupta, Lakmal D. Seneviratne, *Member, IEEE*, Kaspar Althoefer, *Member, IEEE*

***Abstract*—This paper describes the design and construction of a miniaturized triaxial force sensor which can be applied inside a magnetic resonance imaging (MRI) machine. The sensing principle of the sensor is based on an optical intensity modulation mechanism that utilizes bent-tip optical fibers to measure the deflection of a compliant platform when exposed to a force. By measuring the deflection of the platform using this optical approach, the magnitude and direction of three orthogonal force components (F_x, F_y, and F_z) can be determined. The sensor prototype described in this paper demonstrates that it can perform force measurements in axial and radial directions with working ranges of +/- 2 N. Since the sensor is small in size and entirely made of nonmetallic materials, it is compatible with minimally invasive surgery (MIS) and safe to be deployed within magnetic resonance (MR) environments.**

Fig. 1. Miniaturized triaxial optical fiber force sensor prototype.

I. Introduction

MINIMALLY invasive surgery (MIS) is known as a surgical technique that is performed through small incisions with specially designed equipment. An endoscopic camera, which is usually inserted through one of the incisions to provide vision of the operating field, is used together with other surgical tools to perform various specific tasks such as tissue manipulation, retraction, dissection, and suturing. In MIS, the number and size of the incisions are minimized to reduce pain, blood loss, risk of possible infection, and recovery time. For most cases, two to five incisions of 5-15 mm are made to allow surgical interventions within the abdomen. Advance techniques such as single-port laparoscopic surgery [1] and MIS conducted with the aid of magnetic resonance imaging (MRI) [2] have also been developed for even further reduction of required incisions.

The growth of MRI technology offers several benefits to MIS. Not only could the surgical invasiveness be reduced, but also the ability to visualize internal structures of organic tissues is introduced, allowing several complex surgical operations to be performed deep inside an organ [2]. According to such advancement, MRI-compatible robotic systems have also been developed for accommodating surgical procedures that require high maneuverability and accuracy. However, the strong magnetic fields, switching magnetic field gradients, and radio frequency (RF) pulses generated by MRI machines still present large barriers in the development of MRI-compatible robotic equipment. Many conventional robotic parts cannot be utilized and most of them need to be completely re-designed. Sensors and actuators which contain ferromagnetic metal parts (made of, e.g., steel, nickel, or cobalt) cannot be used since they greatly disturb the magnetic field of an MRI machine. Para- and diamagnetic parts (made of, e.g., aluminum, titanium, copper, brass, or lead) do not cause severe problems but they should be carefully used since they could disturb the homogeneity of the magnetic field, causing artifacts in the acquired images. Apart from such difficulties, the lack of force feedback, which is one of the major problems of MIS, also needs to be solved [3].

Force feedback is, in particular, important for MIS since it provides the ability to gain force information when the surgical tool comes in contact with tissue. Conducting the surgery without such a sensing capability could lead to high risks of unexpected tissue damage, blood loss, and trauma. In order to overcome such problems, various sensing techniques have been proposed [3]. These include the optical-based sensing which is key to MRI-compatible force measurement.

The development of optical-based force sensors was earlier demonstrated by Tada *et al*. with the design of a multi-axis force sensor utilizing optical fibers together with a flexible structure [4]. In this case, forces were measured through the modulation of the light intensity. When the

Manuscript received September 15, 2009. The research leading to these results has received funding from the European Community's Seventh Framework Programme (FP7/2007-2013) under Grant Agreement No. 231640.

P. Puangmali, L. D. Seneviratne, K. Althoefer, are with the Department of Mechanical Engineering, King's College London, Strand, London WC2R 2LS, U.K. (e-mail: pinyo.puangmali@kcl.ac.uk; lakmal.seneviratne@kcl.ac.uk; k.althoefer@kcl.ac.uk).

P. Dasgupta is with the Department of Urology, King's College London, Guy's Hospital, London SE1 9RT, U.K. (email: prokarurol@gmail.com).

forces deflect the mechanical structure, the intensity of the light passing from a transmitting fiber to an array of receiving fibers changes, allowing the force magnitudes to be determined. Based on the concept of light intensity modulation, Chapuis *et al*. also described a sensor for torque measurement using optical fibers with a flexible structure and a mirror [5]. Due to the advantage of being a compact sensing structure which is easy to miniaturize for uses in MIS, a number of force sensor prototypes having uniaxial and multiaxial sensing capabilities have successfully been developed [6], [7]. Focusing on the optical-based force measurement, this paper describes the sensing methodology and design of a miniaturized optical fiber force sensor which is derived from our previous work on the development of a force sensitive wheeled probe [6] and a 3-axis optical fiber force sensor for applications in magnetic resonance (MR) environments [8]. As depicted in Fig. 1, the proposed sensor integrated with a distal wheel is to be used to measure tissue hardness and detect areas of tissue abnormality (e.g. tumors or cancers) during MIS.

II. Sensor Design

A. Sensing Principle

The proposed miniaturized optical fiber force sensor operates based on the sensing principle that force is measured by the modulation of the light intensity. As shown in Fig. 2, the intensity modulation mechanism of the sensor consists of two pairs of identical bent-tip optical fibers; the reference fiber pair and the sensing fiber pair. Each fiber pair comprises a set of transmitting and receiving fibers which guide a light signal from a light source to an optical detector via a reflector. The reflector of the reference fiber pair is supported by a rigid stationary structure whereas the reflector of the sensing fiber pair is attached to a flexible structure—the flexure. In case that a force is applied to the sensor, the flexure will deflect. The reflector which is affixed to the flexure will then move away from its original position varying the distance between itself and the fiber tips. Such a movement of the reflector varies the amount of the light reflected to the receiving fiber of the sensing fiber pair. This, then, results in a change of the light intensity measured at the optical detector. At the optical detector, the light signal is converted into an electrical signal and eventually processed to determine the magnitude and direction of the applied force by comparing it to a signal obtained form the reference fiber pair.

The deployment of bent-tip optical fibers as a part of the intensity modulation mechanism is found to be an effective means to modulate the light signal intensity since the most concentrated part of the light beam can be projected from the transmitting fiber core to the core of the receiving fiber [9]. In this configuration, the angle between the fiber tips is considered a key factor that greatly influences the performance of the sensing structure. To achieve the highest possible sensing ability, this angle is optimized through a simulation process which involves the mathematical modeling of the sensing mechanism undergoing changes of the reflector's position and orientation.

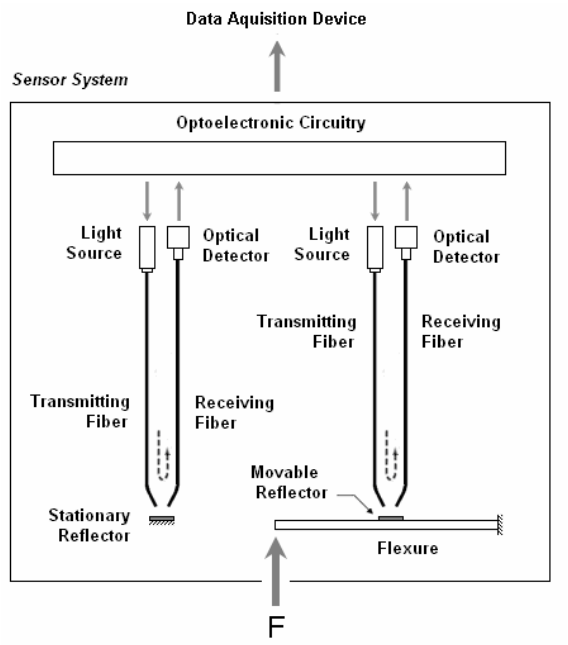

Fig. 2. Schematic diagram of an intensity modulation mechanism that utilizes a reference fiber pair (left) and a sensing fiber pair (right) to perform force measurement.

B. Mathematical Model

The mathematical model of the sensing structure that makes use of bent-tip optical fibers can be formulated by considering the geometry of its fundamental components [8], [9]. As depicted in Fig. 3, the transmitting and receiving fibers, which have an equal core diameter of d and the same numerical aperture (NA), are placed at an angle α with reference to each other, leaving a distance of a between the fiber tips. The reflector is initially located at its original position (horizontal dashed line) that causes a virtual object known as a virtual transmitting fiber. This virtual fiber appears to project a light beam straight to the receiving fiber tip. A change of the distance between the fiber tips and the reflective surface of the reflector causes an offset as well as a change of the distance between the tips of the virtual transmitting fiber and the receiving fiber. In case that the reflector moves from its initial position h to a new position $h+\Delta h$, the virtual transmitting fiber will be displaced with a vertical displacement of $2\Delta h$. Such a movement of the reflector results in an offset of $2\Delta h\sin(\alpha/2)$ between the virtual transmitting fiber and the receiving fiber. The distance between the receiving fiber and the virtual transmitting fiber tip, $\overline{AG}$, can be determined by considering ΔABC

$$\begin{aligned}\overline{AG} &= \overline{AC} - \overline{GC} \\ &= \frac{2(h+\Delta h) + d\sin(\alpha/2)}{\cos(\alpha/2)} - 2\Delta h \sin(\frac{\alpha}{2})\tan(\frac{\alpha}{2}) \\ &= 2(h+\Delta h)\sec(\frac{\alpha}{2}) + d\tan(\frac{\alpha}{2}) - 2\Delta h \sin(\frac{\alpha}{2})\tan(\frac{\alpha}{2}).\end{aligned} \tag{1}$$

The diameter of the projected light circle can be estimated by

$$\begin{aligned}D &= d + 2\overline{AG}\tan\theta \\ &= d + 4(h+\Delta h)\sec(\frac{\alpha}{2})\tan\theta \\ &\quad + 2d\tan(\frac{\alpha}{2})\tan\theta - 4\Delta h \sin(\frac{\alpha}{2})\tan(\frac{\alpha}{2})\tan\theta,\end{aligned} \tag{2}$$

where θ represents the radiation angle of the optical fiber, $\theta = \sin^{-1}(NA)$. The relation between h and a can be derived as

$$\begin{aligned}a &= \overline{EF}\sin(\frac{\alpha}{2}) - d\cos(\frac{\alpha}{2}) \\ &= \frac{2h + d\sin(\alpha/2)}{\cos(\alpha/2)} \cdot \sin(\frac{\alpha}{2}) - d\cos(\frac{\alpha}{2}) \\ &= 2h\sec(\frac{\alpha}{2})\sin(\frac{\alpha}{2}) + d\tan(\frac{\alpha}{2})\sin(\frac{\alpha}{2}) - d\cos(\frac{\alpha}{2}) \\ h &= \frac{a}{2}\cot(\frac{\alpha}{2}) - \frac{d}{2}\sin(\frac{\alpha}{2}) + \frac{d}{2}\cos^2(\frac{\alpha}{2})\csc(\frac{\alpha}{2}).\end{aligned} \tag{3}$$

The intensity distribution of the projected light beam is approximated by a Gaussian function in a polar coordinate as

$$I(r) = I_o e^{-\frac{r^2}{(w/2)^2}}, \tag{4}$$

where r is the radial distance of the projected light beam, I_o is the maximum intensity of the projected light beam, and w is the Gaussian width at *1/e* of the peak. Based on this approximation, the total light flux "virtually" projected out of the virtual transmitting fiber ϕ_t can be calculated as

$$\phi_t = \int_0^{D/2} I(r)\cdot 2\pi r\,dr \approx \int_0^{\infty} I_o e^{-\frac{r^2}{(w/2)^2}} \cdot 2\pi r\,dr = \frac{\pi}{4} w^2 I_o. \tag{5}$$

The total emitted light flux remains the same at any distance away from the tip of the virtual transmitting fiber but the intensity distribution profile of the light changes. This is because of the change of maximum intensity ΔI_o and the change of Gaussian width Δw of the projected light beam—as the distance increases, the maximum intensity of the projected light beam decreases while the Gaussian width increases. Based on (5), this can be mathematically expressed as

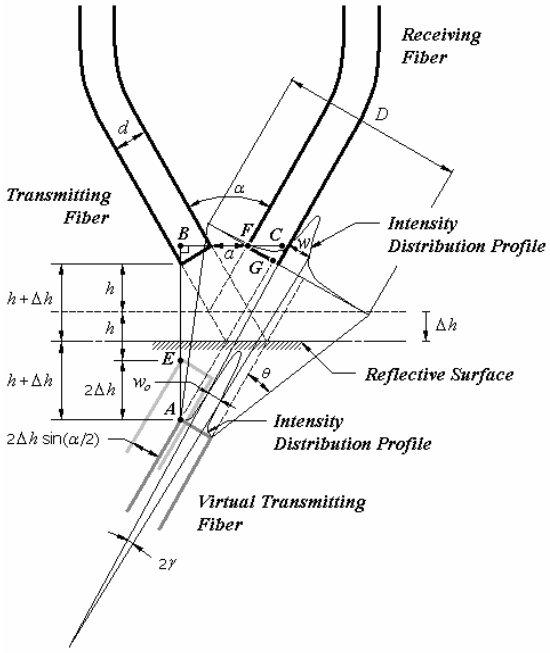

Fig. 3. Geometry of the fundamental components of an intensity modulation mechanism that makes use of bent-tip optical fibers to perform optical intensity modulation with a linearly moving reflector.

$$\frac{\pi}{4}(w_o + \Delta w)^2 (I_o^{'} - \Delta I_o) = \frac{\pi}{4} w_o^2 I_o^{'} \tag{6}$$

or

$$\Delta I_o = I_o^{'} - \frac{w_o^2 I_o^{'}}{(w_o + \Delta w)^2} = I_o^{'} - \frac{w_o^2 I_o^{'}}{w^2} = I_o^{'} - I_o, \tag{7}$$

where

$$w = w_o + \Delta w \tag{8}$$

and

$$I_o = \frac{w_o^2 I_o^{'}}{w^2}. \tag{9}$$

Note that w_o is the Gaussian width of the light beam emitted from the virtual transmitting fiber end face and $I_o^{'}$ is the maximum intensity of the light emitted from the virtual transmitting fiber end face. In relation to a change of the reflector position, the Guassian width can be defined as

$$\begin{aligned}w &= w_o + 2\overline{AG}\tan\gamma \\ &= w_o + 4(h+\Delta h)\sec(\frac{\alpha}{2})\tan\gamma \\ &\quad + 2d\tan(\frac{\alpha}{2})\tan\gamma - 4\Delta h \sin(\frac{\alpha}{2})\tan(\frac{\alpha}{2})\tan\gamma.\end{aligned} \tag{10}$$

In fact, because the tip of the receiving fiber is smaller than the circular pattern of the projected light beam, the light flux that can be coupled into the receiving fiber ϕ_r is smaller

than that determined by (5). The theoretical model of the light flux collected by the receiving fiber is shown in Fig. 4. This model can be written in relation to Δh as

$$(\phi_r)_{th} = 2I_o \int_{-d/2}^{d/2} \int_{0}^{\sqrt{(\frac{d}{2})^2 - x^2}} e^{-\frac{(x \pm 2\Delta h \sin(\alpha/2))^2 + y^2}{(w/2)^2}} dydx. \quad (11)$$

(The offset term could be either positive or negative depending on its definition concerning the direction; however, both lead to the same integral result, thanks to the symmetry of the Gaussian function). When taking into account the inclination of the reflector that causes a shift of the central position of the projected light beam δ, (11) becomes

$$(\phi_r)_{th} = 2I_o \int_{-d/2}^{d/2} \int_{0}^{\sqrt{(\frac{d}{2})^2 - x^2}} e^{-\frac{(x \pm (2\Delta h \sin(\alpha/2) \pm \delta))^2 + y^2}{(w/2)^2}} dydx, \quad (12)$$

$$\begin{aligned} \delta &= \frac{\overline{AG}}{2} \tan(2\beta) \\ &= (h + \Delta h) \sec(\frac{\alpha}{2}) \tan(2\beta) \\ &\quad + \frac{d}{2} \tan(\frac{\alpha}{2}) \tan(2\beta) - \Delta h \sin(\frac{\alpha}{2}) \tan(\frac{\alpha}{2}) \tan(2\beta) \end{aligned} \quad (13)$$

where β represents the reflector inclination angle. (Note that the effect of a small reflector inclination angle is usually insignificant and can be neglected for simplicity.)

In practice, due to imperfect conductivity of the receiving fiber, a lesser amount of the light flux can be actually collected. Also, not all of the collected light traveling through the receiving fiber will finally strike the active region of the optical detector to generate the electrical output [9]. These conditions lead to the modification of (12) as

$$\phi_r = 2\sigma_r I_o \int_{-d/2}^{d/2} \int_{0}^{\sqrt{(\frac{d}{2})^2 - x^2}} \eta e^{-\frac{(x \pm (2\Delta h \sin(\alpha/2) \pm \delta))^2 + y^2}{(w/2)^2}} dydx, \quad (14)$$

where σ_r represents the losses in the receiving fiber including the optical loss due to fiber surface contamination and bending, and η is a Gaussian function having a Gaussian width of c at *1/e* of its peak,

$$\eta = e^{-\frac{x^2 + y^2}{(c/2)^2}}. \quad (15)$$

This function can, however, be omitted if a proper coupling between the receiving fiber and the optical detector is made; otherwise, depending on the intensity of the light entering the receiving fiber, its wavelength, power distribution among all modes of the light beam, and the characteristics of the optical detector, the Gaussian width of this Gaussian function changes, converting the intensity distribution pro-

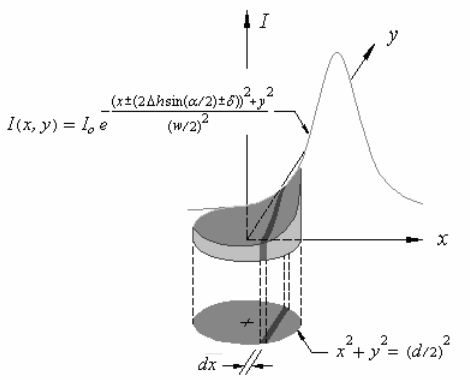

Fig. 4. Model of the theoretically collected light flux. (The intensity distribution profile is bounded by the circular cross-section of the receiving fiber.)

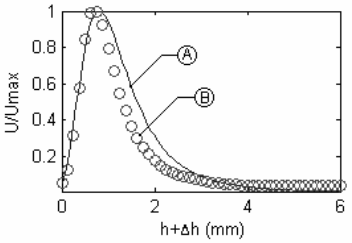

Fig. 5. Simulated (A) and measured (B) responses of a typical intensity modulation mechanism that uses 0.5-mm-diameter bent-tip polymer optical fibers and a flat ABS (Acrylonitrile Butadiene Styrene) plastic plate as a reflector. (The model parameters are a = 1 mm, α = 60°, β = 0°, w_o = 0.2 mm, γ = 0.302 rad, and c = 0.884 mm.)

file of the collected light flux model to the profile of the approximated effective light flux model that, in turn, generates electrical output U at the optical detector,

$$\begin{aligned} U &= k_v \phi_r \\ &= 2k_v \sigma_r I_o \int_{-d/2}^{d/2} \int_{0}^{\sqrt{(\frac{d}{2})^2 - x^2}} e^{-\frac{x^2 + y^2}{(c/2)^2}} \cdot e^{-\frac{(x \pm (2\Delta h \sin(\alpha/2) \pm \delta))^2 + y^2}{(w/2)^2}} dydx, \end{aligned} \quad (16)$$

where k_v is the transforming factor that converts the total light flux arrived at the optical detector into the electrical output. The electrical output values obtained from (16) can be normalized by the maximum output value to create a unitless mathematical model which does not depend on optical losses as follows:

$$\frac{U}{U_{\max}} = \frac{I_o \int_{-d/2}^{d/2} \int_{0}^{\sqrt{(\frac{d}{2})^2 - x^2}} e^{-\frac{x^2 + y^2}{(c/2)^2}} \cdot e^{-\frac{(x \pm (2\Delta h \sin(\alpha/2) \pm \delta))^2 + y^2}{(w/2)^2}} dydx}{\max\left(I_o \int_{-d/2}^{d/2} \int_{0}^{\sqrt{(\frac{d}{2})^2 - x^2}} e^{-\frac{x^2 + y^2}{(c/2)^2}} \cdot e^{-\frac{(x \pm (2\Delta h \sin(\alpha/2) \pm \delta))^2 + y^2}{(w/2)^2}} dydx \right)} \le 1. \quad (17)$$

Fig. 5 demonstrates a normalized model-simulated curve (generated based on (17)) that estimates the real response of a typical intensity modulation mechanism. As can be seen, the response of the sensing mechanism is not monotonic since it possesses both positive and negative slopes. For sensor design, selecting an appropriate operating interval is important to guarantee consistent measurement readings, good sensitivity, and largest possible linear range. Based on the above key aspects, the sensing mechanism of the proposed sensor prototype has been designed for an operation around the position that shows the highest negative slope.

III. Sensor Prototype

A. Sensor Head

The sensor prototype shown in Fig. 6 comprises five major elements; three pairs of sensing fibers, a movable reflector, and a compliant platform. All of the sensing fiber pairs are symmetrically organized on a stationary plastic support, allowing the tip of every fiber pairs to make the same radial distance from the central axis of the sensor. The sensing fibers and the support constitute the sensor's upper part.

The lower part of the sensor is composed of a 3-degree-of-freedom (3-DOF) compliant platform and a circular flat ABS (Acrylonitrile Butadiene Styrene) plastic plate which functions as a reflector of the sensing fibers. The compliant platform is made of polycarbonate—a material that offers good stiffness characteristic, low hysteresis, high impact strength, high corrosion resistance, and good dielectric properties. This platform connects the sensor's upper part to the reflector, enabling an appropriate distance between the reflector and the tips of the sensing fibers to maximize the sensing ability of the sensor. Fig. 6 also shows the design of the compliant platform which comprises three identical flexible beams symmetrically arranged around the central axis of the platform. By employing a manufacturing process using standard machine tools, all beams were fabricated in a monolithic form. If the compliant platform undergoes an axial force load, all three beams will be equally deformed whilst; if a radial force load is applied, the beams will deform differently. The compliant platform is the largest component of the sensor. It forms the sensor head with a diameter of 10 mm. The sensor head can be integrated with a special purpose tool such as a surgical knife or indentation wheel. Fig. 6 shows the sensor integrated with a surgical shaft and a distal peripheral device—a Teflon wheel which enables continuous tissue palpation and rolling indentation to be carried out during MIS [6].

B. Optoelectronics

In this prototype, the optical fibers employed are 0.5-mm-diameter polymer optical fibers which have a core reflective index of 1.492, a cladding reflective index of 1.402, a numerical aperture of 0.51, and a minimum bend radius of 12.5 mm. The tips of the transmitting and receiving fibers are separated by a distance of 1 mm and the angle between the

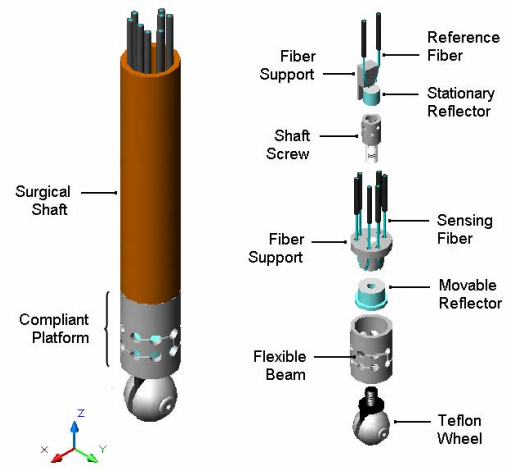

Fig. 6. Enlarged and exploded views of the sensor.

fiber tips is set to 60° such that good measurement sensitivity can be obtained without too much violating the minimum bend radius of the fibers. The light sources that supply light to all the transmitting fibers are high-intensity red LEDs (SFH756V). The LEDs are connected in series with a single current source regulator (L200C) which supplies a constant current to all the LEDs. The optical detectors used to measure the light intensity at the ends of the receiving fibers are photodiodes (SFH250V).

C. Signal Processing

The photodiode of the sensor system operates in a photovoltaic mode—the photodiode together with a precision operational amplifier (OPA111) generates a primary electrical output signal in proportion to the incident light. In this mode of operation, the photodiode offers very sensitive and low noise response to the optical signal delivered by the optical fiber. After the primary electrical signal is generated, it is then further amplified by a standard operational amplifier (LM741) which is arranged in a non-inverting configuration. This secondary amplifier allows the signal level to be adjusted to an appropriate range.

Because the sensor prototype performs its measurement based on optical signal intensity modulation, the variation of the signal intensity can occur due to not only a force applied to the sensor head, but also some uncertainties such as the drift of the light source, the reflectivity degradation owing to the aging of the reflector, and the optical attenuation owing to fiber bending and coupling losses. To cope with these unwanted effects, a reference fiber pair with an ABS reflector is included in the sensor system (see Fig. 6). The reference fiber pair, its light source, and its optical detector are identical to the respective elements of the sensing fiber pairs. The reflector of the reference fibers is, however, affixed to a rigid support keeping the distance between the reference fiber tips and the reflector constant. This distance is set such that the highest level of light flux enters the re-

ceiving fiber. Based on (17), the ratio of the output signal obtained from the optical detector of each sensing fiber pair and that obtained from the optical detector of the reference fiber pair determines the sensor output response which is independent of the described uncertainties.

IV. Calibration

In order to evaluate the sensing characteristics of the force sensor, the sensor (without a distal peripheral device) was initially tested and calibrated with a set of loading masses. To perform the calibration, the sensor was mounted in a particular orientation on a rigid stationary support. It was then loaded with increasing forces at 0.28 N increments until a maximum loading force of approximately 2 N was reached. At each force increment, the difference between the instantaneous normalized output responses and the normalized output responses at no load ($\Delta U/U_{max}$) were recorded. The same calibration procedure was repeated with the sensor mounted in other orientations. Fig. 7 shows the output responses of the sensor. During the calibration, the sensor signals exhibited a maximum peak-to-peak noise of 25 mV. This noise level limits the sensor resolution to approximately 0.05 N.

The record of the sensor outputs acquired from the calibration process was used to derive a calibration matrix which was formulated based on approximated linear relationships over designed working ranges. This matrix mathematically represents the characteristics of the sensor as

$$[F_x \quad F_y \quad F_z]^T = A \cdot [u_1 \quad u_2 \quad u_3]^T \tag{18}$$

or

$$[u_1 \quad u_2 \quad u_3]^T = A^{-1} \cdot [F_x \quad F_y \quad F_z]^T, \tag{19}$$

where $[F_x \quad F_y \quad F_z]^T$ is the force vector, $[u_1 \quad u_2 \quad u_3]^T$ is the output vector of the sensor, and A is the 3 × 3 calibration matrix which relates the sensor output readings to the three orthogonal force components. By applying the linear least square method that linearly correlates the loading forces (F_x, F_y, F_z) to the sensor outputs (u_1, u_2, u_3), each element of the calibration matrix was evaluated. This determines the sensitivity matrix S as

$$S = A^{-1} = \begin{bmatrix} -2.347 & -7.632 & 7.314 \\ 7.692 & 2.260 & 7.066 \\ -5.272 & 4.438 & 6.417 \end{bmatrix} \times 10^{-2}. \tag{20}$$

V. Conclusion

This paper presents the design of a miniaturized optical fiber force sensor prototype developed to realize force feedback capability in MIS. The sensor makes use of an optical sensing scheme with bent-tip optical fibers, reflectors, and a 3-DOF compliant platform to perform force measurement. Since the sensor is entirely manufactured from nonmetallic materials and performs its sensing function without the use of electrical signal at the sensor head, it is suitable to be deployed within the magnetic workspace of an MRI machine. These specialties, then, permit MRI-guided MIS to be performed with the aid of possible force feedback.

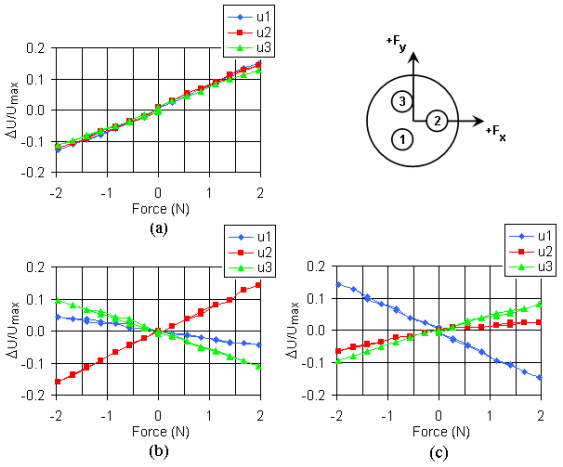

Fig. 7. (a) Measured output responses of the sensor to axial loading/unloading along *z*-direction. (b) Measured output responses of the sensor to radial loading/unloading along *x*-direction. (c) Measured output responses of the sensor to radial loading/unloading along *y*-direction. (Low hysteresis is observed in all cases. The upper right diagram shows the positions of sensing fiber pairs 1, 2, and 3 with reference to force loading directions.)

References

[1] J. H. Kaouk and R. K. Goel, "Single-port laparoscopic and robotic partial nephrectomy", *European Urology*, vol. 55, no. 5, pp. 1163-1170, May 2009.

[2] M. Hashizume, "MRI-guided laparoscopic and robotic surgery for malignancies", *Int. J. Clin. Oncol.*, vol. 12, no. 2, pp. 94-98, Apr. 2007.

[3] P. Puangmali, K. Althoefer, L. D. Seneviratne, D. Murphy, and P. Dasgupta, "State-of-the-art in force and tactile sensing for minimally invasive surgery", *IEEE Sensors Journal*, vol. 8, no. 4, pp. 371-381, Apr. 2008.

[4] M. Tada, S. Sasaki, and T. Ogasawara, "Development of an optical 2-axis force sensor usable in MRI environments", in *Proc. of the IEEE Sensors*, vol. 2, 2002, pp. 984-989.

[5] D. Chapuis, R. Gassert, L. Sache, E. Burdet, and H. Bleuler, "Design of a simple MRI/fMRI compatible force/torque sensor", in *Proc. IEEE/RSJ Int. Conf. Intell. Robot. Syst.*, Sendai, Japan, 2004, pp. 2593-2599.

[6] P. Puangmali, H. Liu, K. Althoefer, and L. D. Seneviratne, "Optical fiber sensor for soft tissue investigation during minimally invasive surgery", in *Proc. IEEE Int. Conf. Robot. Autom.*, Pasadena, CA, 2008, pp. 2934-2939.

[7] J. Peirs, J. Clijnen, D. Reynaerts, H. van Brussel, P. Herijgers, B. Corteville, and S. Boone, "A micro optical force sensor for force feedback during minimally invasive robotic surgery", *Sensors and Actuators A*, vol. 115, pp. 447-455, Sep. 2004.

[8] P. Puangmali, K. Althoefer, and L. D. Seneviratne, "Novel design of a 3-axis optical fiber force sensor for applications in magnetic resonance environments", in *Proc. IEEE Int. Conf. Robot. Autom.*, Kobe, Japan, 2009, pp. 3682-3687.

[9] P. Puangmali, K. Althoefer, and L. D. Seneviratne, "Mathematical modeling of intensity-modulated bent-tip optical fiber displacement sensor", *IEEE Trans. Instrum. Meas.*, vol. 59, no. 2, pp. 283-291, Feb. 2010.